

1 Stratification and Mixed Layer Depth around 2 Iceland, characterization and inter-annual 3 variability

4 Angel Ruiz-Angulo ^{1*}, Esther Portela ², Charly de Marez¹, Andreas Macrander³,
5 Sólveig Rósa Ólafsdóttir³, Thomas Meunier ⁴, Steingrímur Jónsson ^{3,5}, and M. Dolores
6 Pérez-Hernández ⁶

7 ¹Earth Science Institute, University of Iceland, 101 Reykjavik, Iceland

8 ²Univ. Brest, Laboratoire d'Océanographie Physique et Spatiale, CNRS, IRD, Ifremer, Plouzané, France

9 ³Hafrannsóknastofnun / Marine and Freshwater Research Institute, Hafnarfjörður, Iceland,

10 ⁴Woods Hole Oceanographic Institution, Woods Hole MA, USA

11 ⁵University of Akureyri, Akureyri, Iceland

12 ⁶Unidad océano y clima, Instituto de Oceanografía y Cambio Global, IOCAG, Universidad de Las Palmas de Gran Canaria,
13 ULPGC, Unidad Asociada ULPGC-CSIC, Las Palmas de Gran Canaria, Spain

14 *Correspondence to:* Angel Ruiz-Angulo (angel@hi.is)

15 ABSTRACT

16 The ocean around Iceland witnesses some of the most important transformations of water masses that drive the global
17 ocean circulation. Here, we analyze 29 years (1990-2019) of quarterly hydrographic section data collected around Iceland.
18 The hydrographic properties around Iceland show important spatial variability. Based on temperature, salinity, and
19 stratification structure, we classified the Icelandic waters in three distinct regions: the South, the North and Northeast
20 regions. The warm and salty Atlantic Waters that dominate the South show the deepest winter mixed layers (~500m) while
21 the North and Northeast show shallower depths (~100m). Based on the decomposition of total stratification into
22 temperature and salinity contributions, we find that, the subsurface stratification is mainly controlled by temperature in the
23 South, by salinity in the Northwest, while in the North, the North Icelandic Irminger Current and East Icelandic Current
24 alternate seasonally, shifting the region between temperature-dominated and salinity-dominated stratification. The
25 interannual variability of the mixed layer and of its thermohaline properties is also large around Iceland. Mixed layer waters
26 were generally colder in the 90's, then warmed until approximately 2015, and became colder again from 2015 to 2018. In
27 the Northeast, a clear multidecadal mixed layer warming trend clearly emerges from the interannual variability as the
28 Atlantic Water progresses northeastward, which is responsible for transforming locally the upper stratification from salinity
29 dominated into temperature dominated, allowing for the formation of deeper mixed layers. This is associated with the
30 "Atlantification" of the Arctic. Elsewhere, we observe density-compensated changes in mixed layer temperature and
31 salinity, without clear trends. This study provides an unprecedented and detailed description of the seasonal to multi-
32 decadal variability of the mixed layer depth and stratification around Iceland, showing links between this regional
33 variability and changing North Atlantic under global warming.

34 **Keywords:** Mixed layer depth, Mixed layer properties, stratification, Ocean warming, Atlantification, Interannual
35 variability

36

38 The Nordic Seas, together with the Irminger Sea and the Iceland Basin, play a crucial role on the Atlantic Meridional
39 Overturning Circulation (AMOC). The Nordic Seas are among the few places on the globe where the formation of deep
40 waters (1000-3000 m depth) occurs during winter deep convection (Petit et al., 2020). The southern end of the Nordic Seas
41 is bounded by the Greenland-Iceland-Scotland Ridge (GISR). The North Atlantic Current (NAC) brings the warm and salty
42 Atlantic Water (AW) northward into the Nordic Seas (Hátún and Chafík, 2018; Østerhus et al., 2019; Hátún et al., 2021).
43 The AW crosses the ridge in three ways (Fig. 1): (i) between Greenland and Iceland, where the Irminger Current (IC) forms
44 the North Icelandic Irminger Current (NIIC) bringing AW that flows clockwise around Iceland (Jónsson & Briem, 2003;
45 Jónsson & Valdimarsson, 2012); (ii) between Iceland and the Faroe Islands (Mauritzen, 1996); and (iii) through the Faroe
46 Shetland Channel (Hansen and Østerhus, 2000; Hansen et al., 2023), contributing up to 48% of the total AW transport. The
47 AW undergoes strong cooling and densification in the Nordic Seas and the Arctic Ocean (Våge et al., 2015, 2018; Pérez-
48 Hernández et al., 2019; Athanase et al., 2020). This modified AW is referred to as Atlantic-origin Overflow Water (AtOW;
49 *e.g.*, Havik et al., 2017; Casanova-Masjoan et al., 2020) and is one of the two sources of Denmark Strait Overflow Water
50 (DSOW; Semper et al. 2019). AtOW travels southward as a mid-depth water mass in the East Greenland Current (Håvik et
51 al., 2017), from where, part of it diverts east and merges with the NIIC northeast of Iceland (Casanova-Masjoan et al.,
52 2020).

53 The transformation of AW into AtOW takes place in different areas of the Nordic Seas: along the Norwegian Current
54 (Håvik et al., 2017), in the Iceland Sea Gyre (Våge et al., 2013), on the eastern side of Greenland, or even -due to its
55 proximity- in the Arctic Basin (Pérez-Hernández et al., 2019). This transformation has different driving mechanisms
56 impacting mixing and convective processes. Wind-stress and sea-ice retreat drive transformation east of Greenland (Våge
57 et al., 2018), sea-ice retreat and heat exchange dominate north of Svalbard (Pérez-Hernández et al., 2019; Athanase et al.,
58 2020), and heat fluxes are the main drivers in the center of Iceland Sea (Våge et al., 2013). Thus, the Nordic Seas region
59 has been previously described as a “mixing pot” (Renfrew et al., 2019), largely responsible for the overall formation of
60 deep overflow water (Lozier et al., 2019). The Nordic Seas are also a large repository of freshwater arising from glacier/river
61 discharge and from the Arctic. This water mass increases buoyancy and is carried southward by the East Greenland Current
62 (EGC). Therefore, it is crucial to fully understand the variability of the upper ocean, where mixed layers (ML) develop and
63 transform these water masses.

64 The Arctic Ocean is warming much faster than the global average, a process known as the “Arctic Amplification”, which
65 is also associated with the “Atlantification” of the Arctic (Polyakov et al., 2017; Dai et al., 2019). Even though the causes
66 are still in debate, there are evident observed consequences of Arctic Amplification, such as a decrease in the extent of
67 seasonal sea-ice (Dai et al., 2019) and a weakening of the cold halocline (Polyakov et al., 2020). Changes in temperature
68 and salinity in the upper ocean modify the upper ocean stratification, which partially controls the mixed layer depth (MLD).

69 The depth and structure of the ML is primarily controlled by local buoyancy forcing, *i.e.*, surface heat loss and freshwater
70 fluxes, which modifies the water density (Kohler et al., 2018). Wind forcing contributes by enhancing turbulent mixing,
71 deepening the ML under certain conditions (Petit et al., 2020). For instance, within the Iceland Basin, wintertime buoyancy
72 loss drives deep convection, shaping the thermohaline properties that influence the lower limb of the AMOC and its
73 variability in the subpolar North Atlantic (Petit et al., 2021). The pre-existing stratification of the water column is
74 responsible for controlling the effect of the surface forcing. Strongly stratified upper layers resist mixing, while weak
75 stratification allows deeper penetration of turbulence and convection mixing (Pierce et al., 1986). Over shorter timescales,
76 on the order of days, the MLD can significantly deepen as a result of the strong wind events with significant wind stress
77 and associated large wave heights (Skylvingstad et al., 2023).

79 The IPCC report indicates with *high confidence* that roughly 40% of the global ocean mean upper ocean stratification
80 has increased about 3.3–6.1% since 1960 due to both ocean warming and high latitude freshening (Tesdal et al., 2018;
81 Yamaguchi and Suga, 2019; Bindoff et al., 2019; Liu et al., 2020; Sallee et al., 2021). Increased stratification is associated
82 with less efficient diapycnal mixing, reducing the exchanges of heat and tracers from the mixed layer into the ocean interior.
83 It has also been observed, with *high confidence*, that the ML is undergoing changes (Bindoff et al., 2019; on Climate
84 Change, IPCC). Particularly, the shallow summertime ML, which is more likely to be affected by global warming, is
85 deepening at a rate of 5 – 10 m per decade (Sallee et al., 2021). Despite the reported global patterns, it has been also
86 acknowledged that regional changes might differ from the global estimates (on Climate Change, IPCC).

87 The warming of the ML and the associated increase in stratification influence biogeochemical processes like
88 phytoplankton blooms and carbon or oxygen sequestration, key components for the Earth’s climate (Olafsson, 2003; Pérez
89 et al., 2021). In the waters surrounding Iceland, the phytoplankton community is closely linked with the water mass
90 properties and hence, an “Atlantification” will replace polar communities with more Atlantic communities (Cerfonteyn et
91 al. 2023). In the Arctic Ocean, north and northwest of Iceland, the early onset of stratification in spring gives rise to rapid
92 shallowing of the mixed layer and triggers early spring phytoplankton blooms, whereas the weakly stratified water-column
93 in the Atlantic water and associated deep ML delays the spring bloom South of Iceland (Zhai et al., 2012). This also has
94 strong consequences in carbon uptake, vertical nutrient supply and biological processes (Yamaguchi and Suga, 2019).
95 Other indirect impacts of the increased stratification include changes in upwelling, deep-water formation rates, biological
96 production, and remineralization rates (Holt et al., 2016), and deoxygenation (Shepherd et al., 2017).

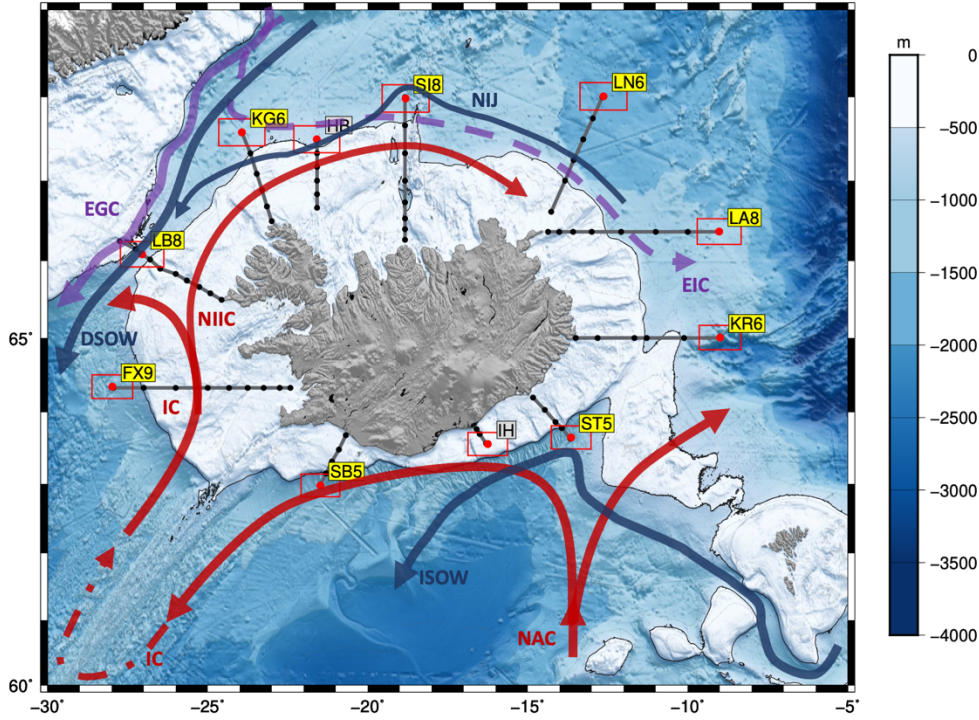
97 At the regional scale, it is challenging to determine the extent to which changes in stratification and in water-mass
98 properties are driven by natural or human-induced variability. Moreover, the relatively short observation records in most
99 of the oceanic regions hinder the attribution of the observed changes to the driving mechanisms and forcings. In this study,
100 by using a long time series of hydrographic observations around Iceland spanning 29 years, we aim at unraveling the
101 different scales of variability of the water-mass properties, MLD, and stratification around Iceland.

102 2 DATA AND METHODS

103

104 We use Conductivity-Temperature-Depth (CTD) data from the repeated hydrographic observational program of the
105 Icelandic Marine and Freshwater Research Institute between 1990 and 2019. The oceanographic surveys took place
106 quarterly, mainly in February, May, August, and November with little coverage during the intermediate months.
107 Observations are made at standard repeated sections. The profiles are obtained with a Seabird 911plus CTD mounted on a
108 rosette with Niskine bottles. The conductivity data are calibrated with salinity samples taken at the bottom of each station.
109 All sensors underwent regular calibrations by the manufacturer.

110 In our analyses we considered only the deepest stations in each section (red dots in Fig. 1), including nearby stations
111 within an area defined by $1^\circ \times 0.5^\circ$ in longitude and latitude (red boxes). The selected stations are located outside of the
112 Icelandic shelf (about 500 m depth). This criterion was chosen to avoid topographic effects, such as across shelf processes
113 on the stratification of the water column and to avoid MLDs limited by shallow bathymetry. Thus, the stations in gray, HB
114 and IH in Figure 1 were not considered as they fall on the shelf. For the sake of simplicity these stations will be named
115 with the acronym of the standard section, first two letters and the station number. The station full name (section and station
116 number) can be found in Table 1.



117
 118 **Figure 1: Map of the typical hydrographic sections collected by the Marine and Freshwater Research Institute around Iceland; the**
 119 **black dots represent the nominal location of the standard stations from 1990-2019. The red dots are the stations used for this analysis**
 120 **and the red boxes delimit the area within which all data were considered for this study. The grey bathymetric contours are spaced**
 121 **every 100 m for the shallow water until the 500 m depth (thick black line) and then every 500 m. The hydrographic stations shown**
 122 **in the yellow boxes corresponding to the standard sections: Faxaflói (FX9), Látrabjarg (LB8), Kögur (KG6), Hornbanki (HB),**
 123 **Siglunes (SI8), Langanes NE (LN6), Langanes E (LA8), Krossanes (KR6), Stokksnes (ST5), Ingólfshöfði (IH) and Selvogsbanki**
 124 **(SB5). The gray labeled IH and HB were not used in this analysis. The main surface and deep currents are also depicted on the map.**

125

126 In this study we analyze the inter-annual variability and linear trends of the ML over a 28-year period as well as the
 127 seasonal variability using the seasonal extremes (summer and winter), when there is more data coverage. From the CTD
 128 stations we estimated the MLD using the density threshold method with a criterion of $\int_{-}\theta = 0.01 \text{ kg m}^{-3}$ (as, for instance,
 129 in Piron et al., (2016) in the Irminger Sea) and a reference depth of 10 m. We chose this criterion instead of the usual 0.03
 130 kg m^{-3} (De Boyer Montegut, 2004) as the latter overestimated the MLD in more than 500 visually inspected profiles (not
 131 shown). For comparison and robustness of our chosen method, we also estimated the MLD using other criteria (de Boyer
 132 Montegut et al., 2004; Holte et al., 2017). However, we found the density threshold method appropriate for our region as it
 133 shows to be effective even for cases where the variations of salinity and temperature were large. Those variations usually
 134 compensate in density making this method more suitable. We have validated our method against previous work by Våge et
 135 al., 2018, where a glider data was available, and the results were satisfactory.

136 For each profile we computed the Brunt -Väisälä frequency (N^2), defined as:

137
$$N^2 = g \frac{1}{\sigma_{-\theta}} \frac{\partial \sigma_{-\theta}}{\partial z}, \quad (1)$$

138 where g is the gravity acceleration, $\int_{-}\theta$ is the potential density and z is depth. N^2 can be decomposed to show the relative
 139 contribution of salinity and temperature to the observed stratification as follows:

140
 141
$$N^2 = N_T^2 + N_S^2, \quad (2)$$

142 where N_T^2 and N_S^2 are the components representing the stratification set by the temperature and salinity, respectively and
143 are defined as:

$$144 N_T^2 = g \left(\alpha \frac{\partial T}{\partial z} \right), \quad (3)$$

145

$$146 N_S^2 = g \left(\beta \frac{\partial S}{\partial z} \right), \quad (4)$$

147 where α is the thermal expansion coefficient and β is the haline contraction coefficient at constant pressure. This
148 decomposition has also been made to classify the oceans by their stratification contribution into α -ocean, β -ocean, and
149 transition zone, where in α -oceans stratification is permanently dominated by temperature, in β -oceans by salinity and the
150 transition regions are either intermittently or seasonally dominated by temperature or salinity (Carmack, 2007; Stewart and
151 Haine, 2016). For the water column to be statically stable, N^2 must be positive. However, the contributions may not be
152 positive; when any of its components, N_T^2 or N_S^2 are negative, temperature or salinity respectively has a destabilizing effect
153 on the resulting stratification that must be compensated by the other variable to maintain a stable water column. Small
154 values of N^2 indicate that the water column is weakly stratified which favors mixing due to winter convection and deeper
155 MLD.

156 To investigate furthermore the driving mechanism of the MLD we used a one-dimensional model (Price et al., 1986)
157 initialized with ERA-5 12-hour dataset of wind stress, heat, and freshwater fluxes (Hersbach et al., 2020) and the
158 summer/winter averaged vertical profiles of temperature and salinity from the observations presented here (see
159 supplementary material). The 1D model would reveal the contribution from diurnal heating/cooling freshwater fluxes and
160 wind mixing. In addition, we broaden the impact of our findings by using the hydrographic database published in Brakstad
161 (2023) that includes, in addition to the dataset from the Marine and Freshwater Research Institute of Iceland, other
162 multiplatform observations like Argo floats or cruise data between 1950 and 2019. For this objective, a larger oceanic
163 region is used and classified into α -ocean and β -ocean using the spice frequency, K^2 , (Carmack, 2007; Strehl et al., 2024),
164 defined as:

$$165 K^2 = N_T^2 - N_S^2. \quad (5)$$

166 K^2 is positive (negative) in α -(β -)oceans.

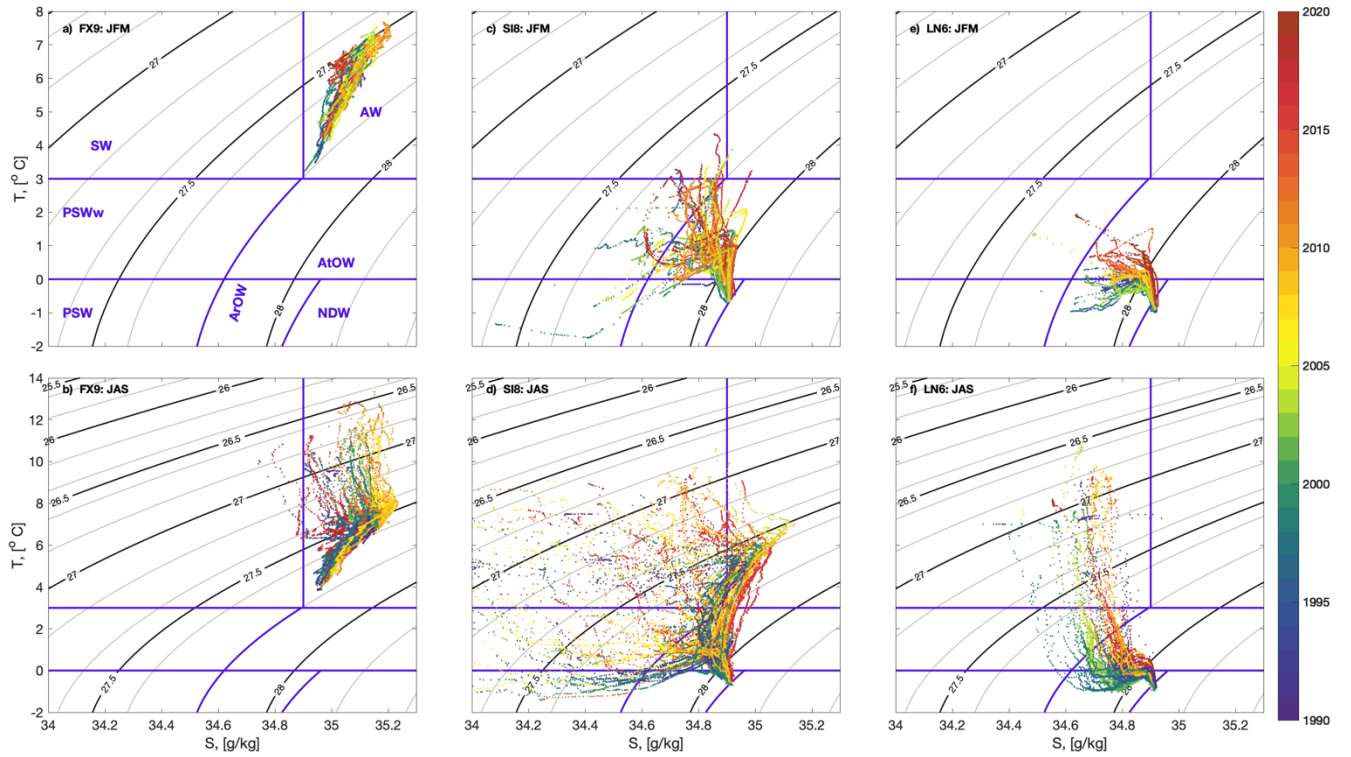
167

168 3 RESULTS

169 3.1 Hydrographic properties around Iceland

170 The hydrographic properties (potential temperature-salinity diagrams) around Iceland show important spatial, seasonal
171 and interannual variability are shown in Figure 2; the T/S properties differ widely between the three representative stations:
172 FX9, SI8 and LN6 for the west, north and northeast of Iceland. FX9, in the southwest of Iceland, is completely dominated
173 by Atlantic Water (AW; Fig. 2 a and b). At SI8, in the North, the dominating water masses in winter are of polar origin,
174 i.e., warm Polar Surface Water (PSWw) in the upper layers, and Atlantic Overflow Water (AtOW) and Arctic Overflow
175 Water (ArOW) in the intermediate/bottom waters (Fig. 2c and d). The SI8 station also presents the largest dispersions of
176 its thermohaline characteristics. It is noteworthy that using fixed definitions of water masses may lead to biased estimates,
177 as these water masses have been steadily warming over the past two decades. LN6, in the Northeast, contains the coldest
178 and densest waters on average (Fig. 2c and f).

179



180
 181 **Figure 2: (Top row) Winter (JFM) and (bottom row) summer (JAS) T-S diagrams for three selected stations (a, b) FX9, (c, d) SI8**
 182 **and (e, f) LN6, considered as representative for the South, North and Northeast regions shown in Fig. 1. The T-S individual**
 183 **profiles are color-coded by year. The main water masses as defined in Table 2, are labeled in panel (a).**

184 The three stations have a clear seasonality. Overall, the summer profiles span a wider temperature range due to seasonal
 185 warming of the upper layers (Fig. 2b, d, f) than in winter (Fig. 2a, c, e). FX9 is notably warmer and saltier than the other
 186 stations, especially in summer (Fig. 2a), when the minimum temperature in FX9 (nearly 4°C) is as high as the maximum
 187 temperature in SI8 and 2 degrees higher than in LN6 (Fig. 2a, b, c). At SI8 a large change in density between seasons is
 188 observed mainly driven by the contribution of AW, explained by offshore migration of the NIIC and the stronger inflow of
 189 AW during the summer (Fig. 2c, and f) (Jónsson and Valdimarsson, 2012). While the widest seasonal amplitude in salinity
 190 is observed at SI8, the largest seasonal amplitude in temperature is observed at LN6.

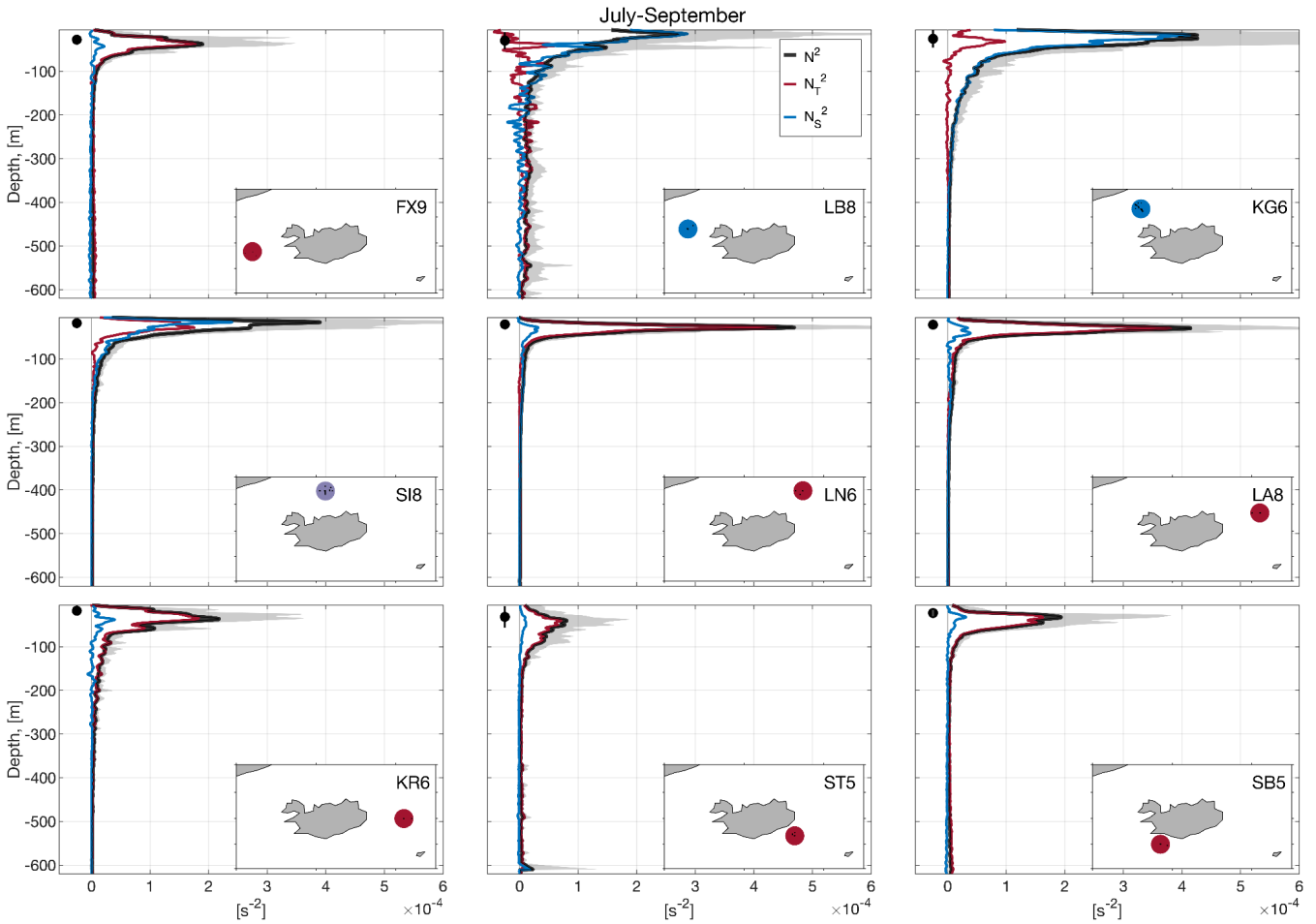
191 FX9 does not show a clear interannual pattern in summer but in winter the 2000's are strikingly saltier than the other
 192 years. In contrast, at SI8 and LN6 fresher and colder waters are observed in the 90's, they progressively warm and become
 193 saltier over time, and they reach their maximum temperature and salinity by 2015-2018. This decadal pattern is more
 194 evident in winter, but it is observed in both seasons.

195 3.2 Seasonality of Stratification and Mixed Layer Depth (MLD)

196 The spatial and temporal variability of the stratification around Iceland is remarkably large (Fig. 3 and Fig. 4), and the
 197 relative contribution of temperature and salinity shows a strong seasonal cycle. In summer, the MLD is relatively shallow,
 198 oscillating around 50 m with a small standard deviation (Fig. 3). In contrast, in winter the ML reaches depths greater than
 199 400 m in FX9, ST5 and SB5 with large standard deviations spanning a 100 m range (Fig. 4). The deepest average MLD is
 200 found in FX9 while the shallowest are KG6, SI8, LA8 and KR6.

201 In summer (Fig. 3), the upper-ocean stratification around Iceland (Fig. 3) is generally dominated by temperature, except
 202 for the three Northwestern stations (namely LB8, KG6, SI8). LB8 exhibits the largest variability in both N_T^2 and N_S^2 , but is
 203 mainly dominated by salinity in the upper 200 m and by temperature below that depth. This transition station is located at

204 the sill of Denmark Strait, a convergence zone for several currents (see Table 1 and Fig. 1) carrying water masses with
 205 contrasting T-S properties within the ML and the thermocline (Jónsson, 1999; Logemann et al., 2013; Casanova-Masjoan
 206 et al., 2020). In KG6, the fresh inflow from the EGC compensates for the cold temperature, and salinity largely dominates
 207 stratification. For SI8, we observe a mixed regime with almost equal contributions from both salinity and temperature to
 208 the total stratification, which suggests that this is also an area of transitional regime. For the stations: LN6, LA8 and KR6,
 209 despite the fact that stratification is mainly dominated by temperature, exhibits a small subsurface contribution of salinity
 210 just below the ML, likely due to the presence of fresh PSWw. The southern stations ST5 and SB5, have a minimal
 211 contribution to stratification from salinity, which may be associated with the numerous river discharges and the proximity
 212 to the continental shelf. The river discharge is the largest near SB5, likely explaining the summer subsurface contribution
 213 to salinity (Whitney, 2025).

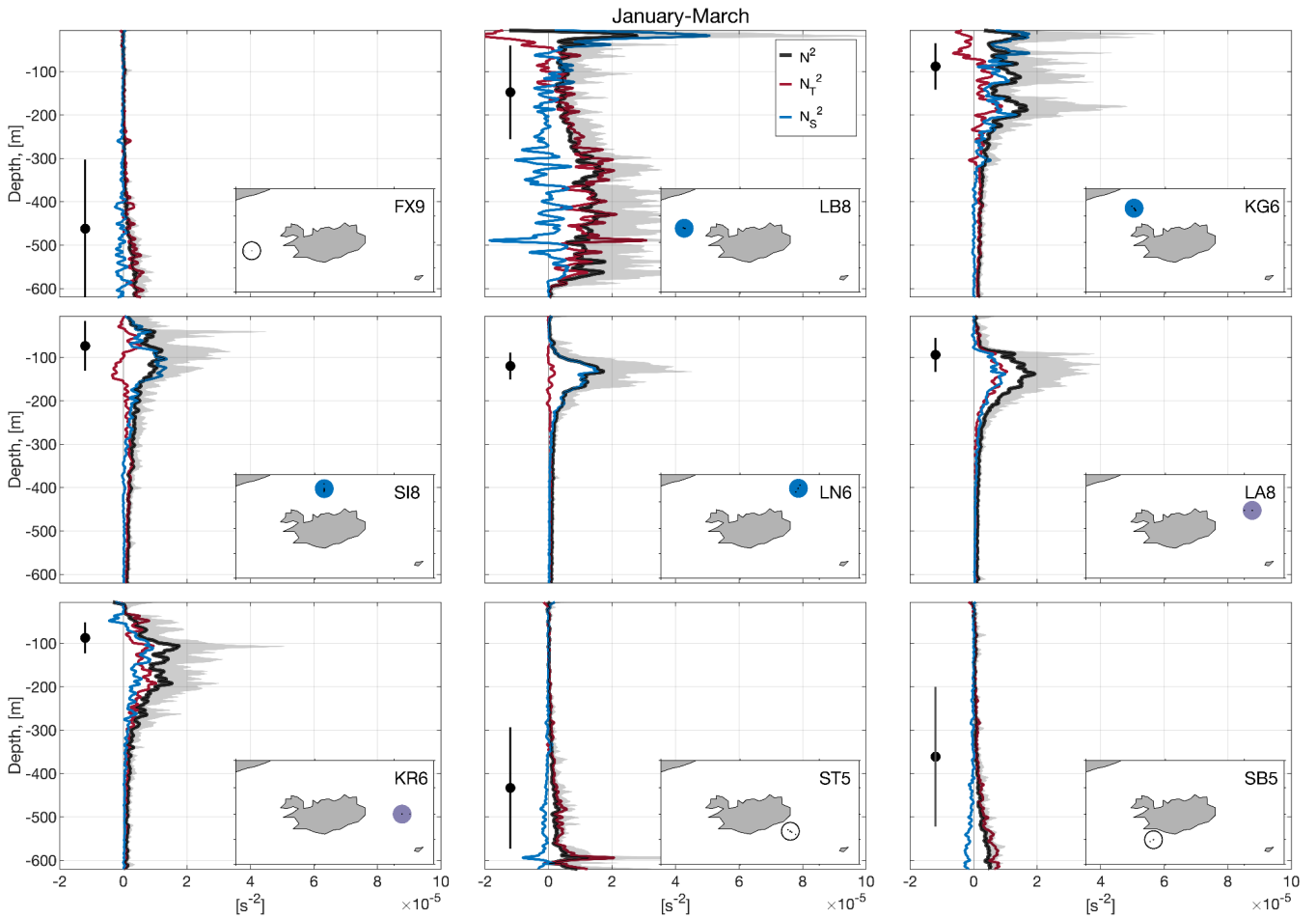


214
 215 **Figure 3: Summer (JAS) average density stratification (N^2) profiles for the selected stations; the average total stratification (black)**
 216 **is decomposed into temperature (red) and salinity (blue) contributions, while the gray shaded band represents all the stratification**
 217 **profiles. The black solid dot (left of the profiles) represents the average MLD with the error bar showing the standard deviation as**
 218 **an indicator of the temporal variability. The maps in the lower corner show the location of the station within a circle color coded by**
 219 **the dominating regime according to the contribution to stratification: red for temperature, blue for salinity, and purple for a mixed**
 220 **regime.**

221 The hydrographic conditions are very different for winter; the stratification is one order of magnitude lower, i.e.,
 222 comparing Figure 3 and Figure 4. Also, the water temperature is much colder due to winter heat loss. Under these
 223 conditions, the relative contribution of salinity to the total stratification stands out around Iceland except at the southern
 224 stations (FX9, SB5, ST5), where the weakest winter stratification is observed. This southern region shows the deepest
 225 MLD, between 350 and 700 m in the stations FX9, SB5 and ST5, while for the northern stations (KG6, SI8, LN6, LA8,
 226 and KR6) the mean winter MLD is about 100 m. Similar to summer, station LB8, also shows high variability in winter

227 stratification, associated with the confluence of currents at the Denmark Strait.

228 The role of temperature or salinity in setting the stratification (α - and β - ocean, see *e.g.*, Carmack, 2007) is linked to the
229 hydrographic characteristics (temperature and salinity) of the dominant water masses within each region. Based on this, we
230 can classify the waters around Iceland. The southern side is an α -ocean as it receives the influence of warm and relatively
231 salty AW. Hence, the stratification is mainly temperature driven in both seasons (see FX9, ST5 and SB5 in Figures 3 and
232 4) and MLD gets deeper than 400 m in winter. The northwest of Iceland (LB8, KG6) is under the influence of the EGC
233 throughout the year bringing fresh PSW and PSWw into the area. Therefore, this area with winter MLDs of 100-150 m can
234 be considered a β -ocean, with heat fluxes equivalent to the southern region but with stronger and salinity dominated
235 stratification blocking the potential for deep convection, i.e., this region does not have a mechanism to lose surface
236 buoyancy seasonally in the salinity component. In contrast, the northeastern Icelandic area (SI8, LN6, LA8 and KR6) shifts
237 from β in winter to a mixed α/β in summer. This is likely due to an offshore migration of the NIIC increasing the inflow of
238 AW (Jónsson and Valdimarsson, 2012; Casanova-Masjoan et al., 2020, their Figure 11). For instance, in winter, SI8 has a
239 PSW signature at the thermocline with salinity driving the stratification and a MLD of about 90 m (β -ocean), and in summer,
240 the NIIC brings warm AW to the upper layers of SI8 making the stratification similarly driven by temperature and salinity.
241 Overall, the north of Iceland exhibits the strongest summer stratification of the study area which results in very shallow
242 MLDs.



243
244 **Figure 4: Same as Figure 3 but for winter (JFM). The white color circles shown in the maps of stations ST5, SB5, and FX9 indicate**
245 **very weak winter stratification with no significant contribution of salinity or temperature.**

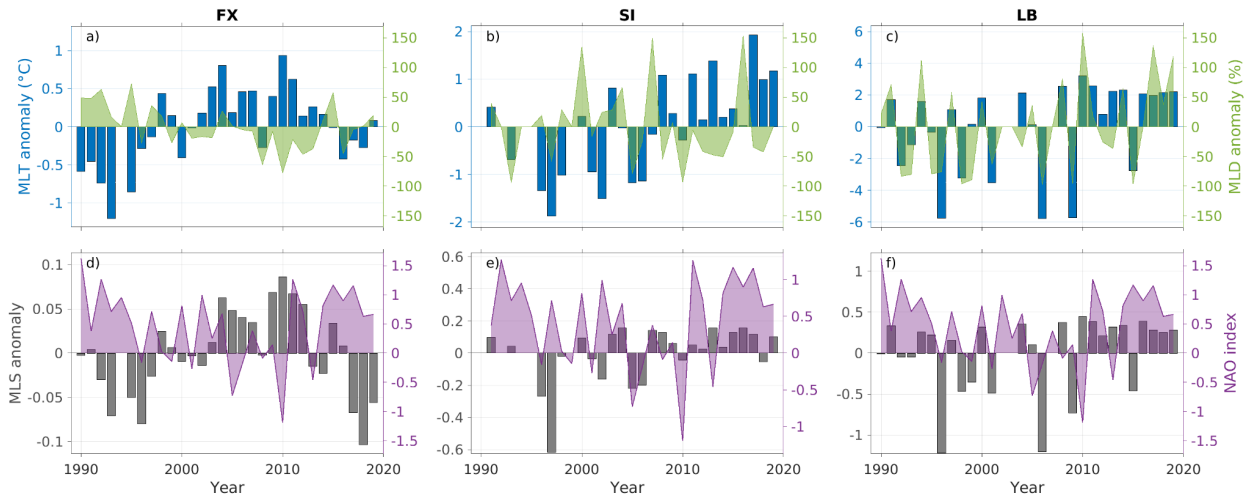
246
247 **3.3 Interannual to decadal variability of the mixed layer properties**

248 To investigate the interannual to decadal ML variability we focused on three reference stations, considered representative
249 of the α -ocean (FX9, West), transition (SI8, North) and β -ocean (LB8, Northwest) regimes around Iceland. FX9 dominated
250 by relatively warm and salty AW, SI8 as a transition area, and LB8 dominated by cold and fresh PSW. The three stations
251 show strong interannual variability.

252 In FX9, to the West of Iceland, there is a correlation ($R=0.69$ p -value <0.01) between mixed layer temperature (MLT)
253 and salinity (MLS) anomalies. Between 1990 and 1998 the mixed layer was the deepest, coldest and second fresher period,
254 as shown in Figure 5a, and d (positive MLD anomalies correspond to deeper ML and negative ones correspond to shallower
255 ML). Around the period 2000-2014, there is an increase in MLT and MLS as the ML becomes moderate shallower. The
256 winter MLD is the shallowest, saltiest, and warmest in 2010 (Fig. 5a, and d), where the temperature contribution seems to
257 control this minimum. From 2015 to 2018 the ML returns to the cold and fresh conditions of the 90's but the MLD is
258 average. The observed variability of the ML and its temperature in FX9 exhibits certain correlation (R) with the NAO; for
259 MLD, the best correlation was $R=0.53$, p -value <0.01 at lag zero; for MLS $R=-0.52$, p -value <0.01 at lag -2 years (NAO
260 leading), and for MLT $R=-0.49$, p -value <0.01 at lag -1 year (NAO leading (Fig. 5g, h). However, we consider that a 2-year
261 lag lacks a realistic physical explanation, thus, we prefer to not to consider this as a reliable correlation. More qualitatively,
262 positive NAO at the beginning and the end of the time series, corresponds with deeper colder and fresher MLs, while
263 negative NAO between 2000 and 2015 roughly corresponds with shallower, warmer, and saltier MLs. As shown in Figure
264 2, FX9 contains only AW (Fig. 2a, d) likely advected from the South to the area by the Gulf Stream and later the Irminger
265 Current. Similar conditions have been observed in the Irminger Sea over the same period, and they have been related to the
266 NAO phase and its impact on the Subpolar gyre (Feucher et al., 2022). This suggests that the FX region is largely influenced
267 by the Atlantic climate and therefore it is partly impacted by the NAO (Bersch, 2002).

268 At SI8, in the North of Iceland (Fig. 5b, e, h), the negative winter MLD anomalies are on the order of those at FX9 and
269 also exhibit strong interannual variability without an identifiable pattern. Strong positive MLD anomalies are observed in
270 particular years (*e.g.*, 2000, 2007, and 2016) but they do not seem correlated with the MLT/MLS or with the NAO
271 variability. Interestingly, the MLT and MLS co-vary during the period 1990-2005, when the mixed layer is colder and
272 fresher, but this correlation weakens from 2005 to 2018, when the positive MLT anomalies increase while the MLS
273 anomalies, although positive, do not vary significantly.

274 In LB8 (Northwest), the winter MLD has the largest variability as the station is located in the vicinity of the front between
275 NIIC and the EGC, which shapes the Polar and Atlantic conditions. Despite this large variability, a co-variance between
276 MLT and MLS anomalies seems to be correlated with the position of the front. Fresher and colder MLs are associated with
277 EGC influence and warmer/saltier MLs with the presence of NIIC (Fig. 5c, f, l). Generally, shallower MLs are also fresher
278 and colder, which agrees with a salinity-dominated stratification in the upper layer (Fig. 4b). Three particular years present
279 relatively deep, cold, and salty MLs: 1996, 2006 and 2014. The observed interannual variability in the ML and its properties,
280 while large, does not seem to be correlated with the NAO, except the last decade where the high state of the NAO is
281 consistent with the positive MLT and MLS, suggesting a larger presence of the NIIC at this station.



284

285

286

287

288

289

290

291

Figure 5: Interannual winter (JFM) variability from 1990 to 2018 in three stations representative of different regions around Iceland. of: (a, b, c) MLD anomaly (in percentage of its mean winter value over the whole record, green shading) and mixed layer temperature (MLT, blue bars). (d, e, f) Mixed layer salinity (MLS, grey bars) and winter average NAO index for comparison (purple shading). The represented stations are (a, d) FX, in the Southwest, (b, e) SI, in the North, and (c, f) LB in the Northwest. Positive anomalies in MLD, MLS and MLT correspond to deeper, warmer and saltier waters, respectively. The summary of the correlations is presented in Table 1.

Table 1: Pearson correlations between different variables. Non significant correlations have been omitted. The shown correlations are significant at 95% confidence ($p < 0.05$), and those significant at 99% ($p < 0.01$) are in bold.

	FX		SI		LB	
	Correlation	p-value	Correlation	p-value	Correlation	p-value
MLT-MLS	R=0.69	p<0.01	R=0.74	P=<0.01	R=0.95	P<0.01
MLT-MLD	-	-	-	-	R=0.76	P<0.01
MLS-MLD	-	-	-	-	R=0.68	P=<0.01
NAO-MLD	R=0.53	P<0.01	-	-	-	-
NAO-MLT	R=-0.41	P<0.03	-	-	-	-
NAO-MLS	-	-	-	-	-	-

292

293

294

295

296

297

298

299

300

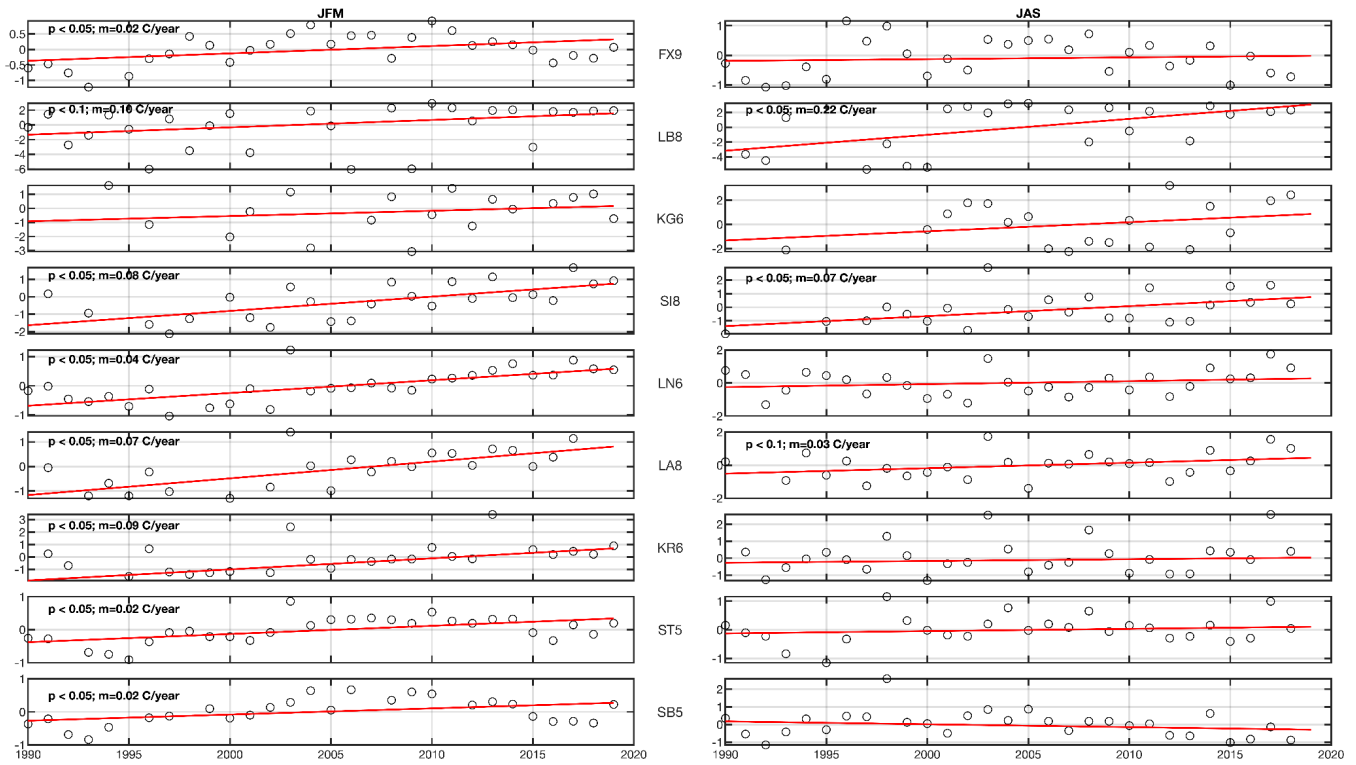
301

302

To delve into the interannual to decadal variability of the MLT around Iceland, we analyzed its anomalies (relative to the long record) in all nine stations and computed their linear trends (Fig. 6). The temperature anomalies show significant interannual variability and spatial differences around Iceland. For instance, positive anomalies were observed in 2003 in most of the stations in both seasons, with particularly large temperature anomalies east of Iceland. Strong warm anomalies are also observed in 2017, mostly in summer at all stations except FX9 and SB5, located South of Iceland (Fig. 6; left panel). Although the 28-years period might be too short for identifying linear anthropogenically-driven trends, linear trends are significant in some of the stations, (where the p-value is indicated). The linear trends show a general warming of the mixed layer that is more evident in winter, mainly in the stations of the northeast (LN6, LA8). In the South (ST5, SB5 and FX9), even if the trend is significant from 2000-2015, there is an interannual variability that induces colder mixed layer conditions from 2015 to 2018. This tendency of returning to the conditions observed in the early 90's may be associated

303 with the NAO (Future et al., 2022) as shown in Fig. 5. The observed general warming of the ML around Iceland is consistent
 304 with the progressive warming of the NIIC (Casanova-Masjoan et al. 2020).

305



306

307

308 **Figure 6: Mixed Layer Temperature (MLT) anomaly time series (left) winter (JFM) and (right) summer (JAS) for the 9 stations**
 309 **shown in Figures 3, 4. The anomalies show the p-values and the linear trends.**

310

4. MLD driving mechanisms from a 1D model

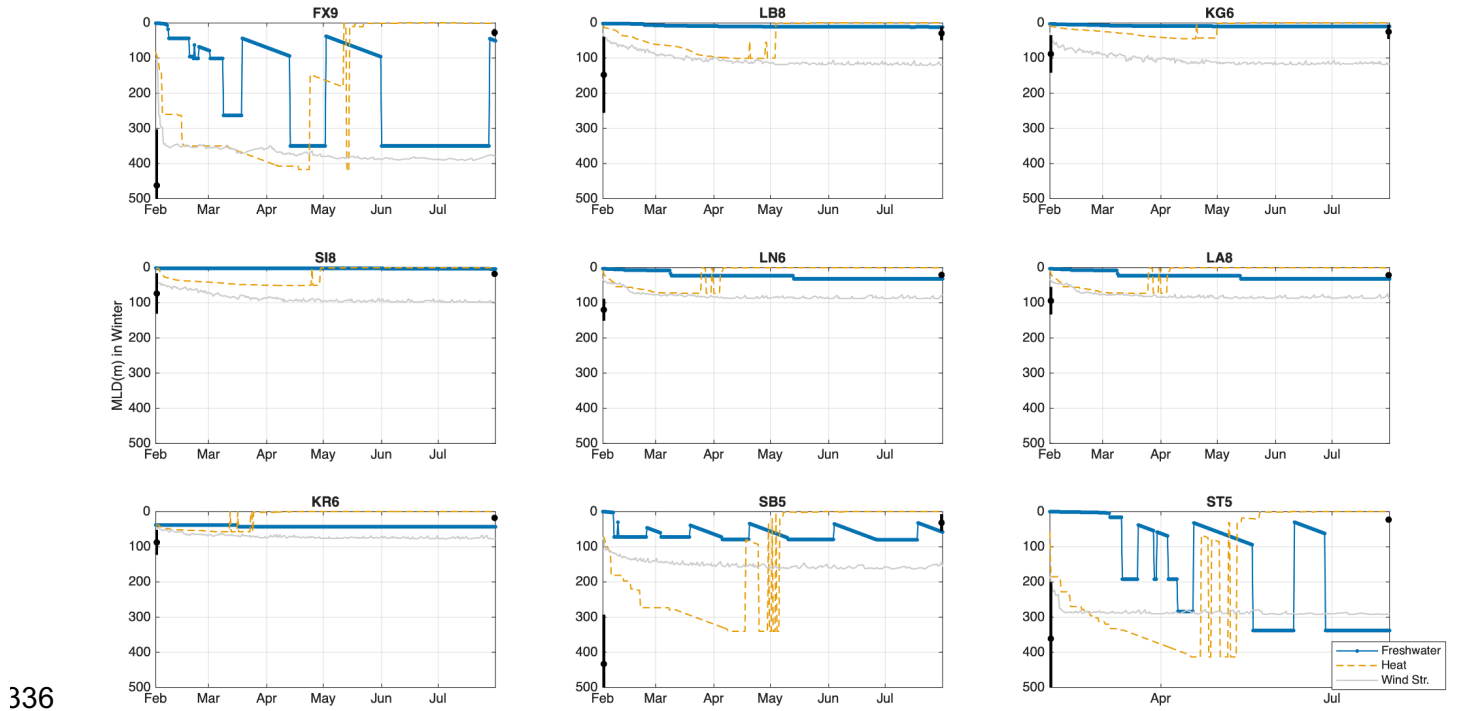
311 The summer stratification around Iceland is an order of magnitude higher than in winter and hence summer MLDs are
 312 very shallow and with higher variability. Therefore, we only use the winter season to study the atmospheric effect on these
 313 α - and β -ocean regions by using the Price et al. (1986) one-dimensional model. It is worth mentioning that the 1D model
 314 estimates the MLD from temperature-based profiles while the estimates from observations are density threshold based. The
 315 MLDs shown in Figure 7 are within the range of the observed average \pm standard deviations (black dots and lines in Figure
 316 7). For all stations a spring shoaling of the MLD is driven by heat flux, while the MLD remains relatively deep due to the
 317 wind-stress. The choice of PWP model was made to support the idea that β - and transition oceans do not develop deep
 318 mixed layers, which is shown in Figure 7.

319 In the model, the stations embedded in AW (SB5 and ST5) present the largest MLDs exceeding 300 m depth, which is
 320 consistent with the observations. In this α -ocean region, the development of a deep ML is driven mainly by heat fluxes
 321 (Fig. 7 h and i), which also holds for FX9. However, wind-stress steadily contributes to the development of the ML (Fig.
 322 7a, h and i). During the summer, shoaling of the mixed layer is likely influenced by the changes of both heat and freshwater
 323 fluxes, with their effects on the MLD partially offset by wind stress (Fig. 7a, h and i).

324 The station LB8, despite being in Denmark Strait and presenting a large contribution of PSWw and PSW in the upper
 325 layers (driving a β -ocean stratification), shows that the development of MLDs can be influenced by both, heat flux and/or
 326 wind stress (Fig. 7b). However, the contribution of wind-stress leads to a slightly deeper MLD than the heat fluxes (Fig.

327 7b). Wind stress becomes the lead forcing mechanism northeast of LB8 (KG6, SI8), coinciding with the shift from α - to β -
 328 ocean stratification (Fig. 7b, c and d). This region represented by LB8 station does not have a large convection potential
 329 compared to those with pure AW and hence do not produce large MLDs (Fig. 4) and the MLD is a result of convection
 330 wind-mixing in roughly equal parts.

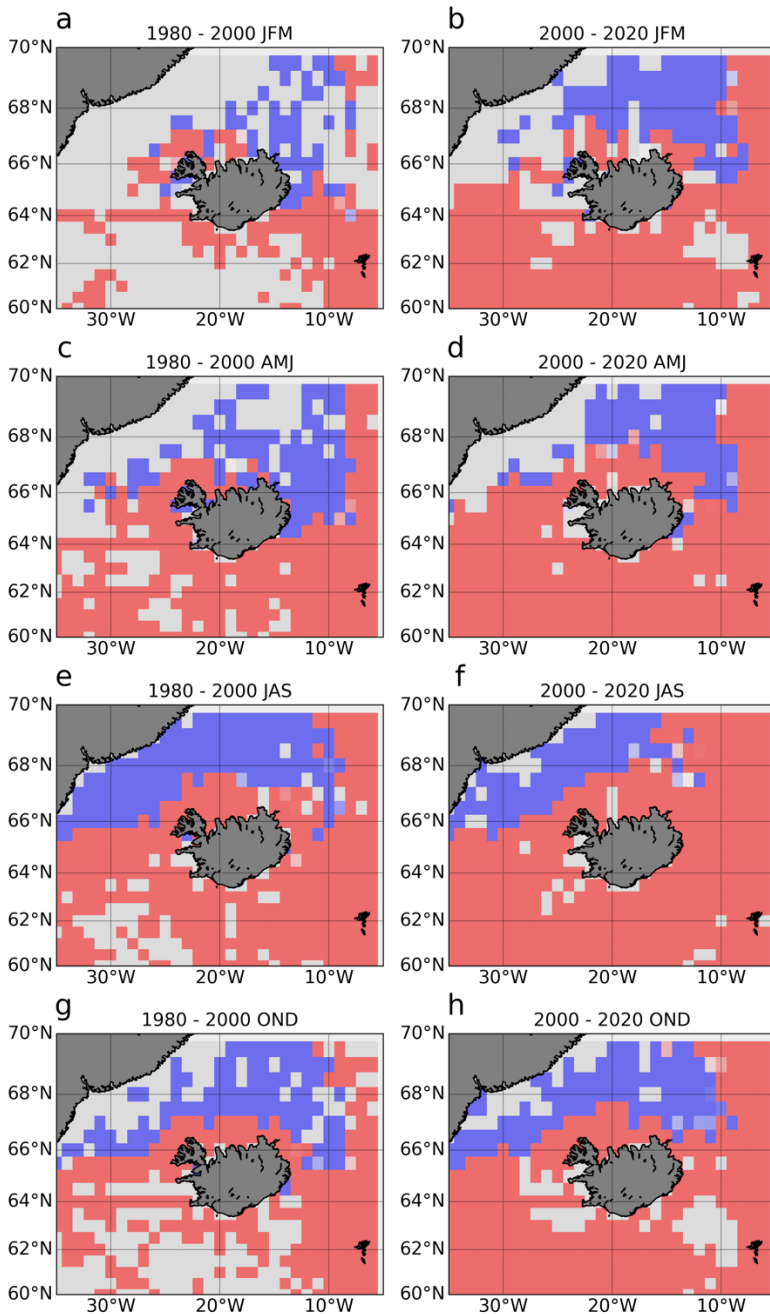
331 At LN6, LA8 and KR6 before spring, wind-stress and heat fluxes contribute similarly to the development of the MLD;
 332 those stations are at the core of the EIC, which contains PSWw in the upper layers and AtOW beneath. Hence the wind-
 333 stress and heat fluxes are the driving mechanisms acting on the water column (Fig. 7e and f). As the wind-stress develops,
 334 the MLD evolution erodes the PSWw strata reaching the AtOW layer, allowing the heat fluxes to lead the MLD
 335 development.



337 **Figure 7: MLD driving mechanism decomposition estimated from the PWP 1-D model (Price et al. 1986) for each of the studied**
 338 **stations. Different MLD evolutions are shown for outputs forced with freshwater fluxes (blue), heat fluxes (red), and wind-stress**
 339 **(green). Black dots represent the averaged winter and summer MLD with their standard deviations.**

340 5. Stratification around Iceland

341 To complement the understanding of the stratification of the Arctic and Subarctic waters around Iceland, their connection
 342 with water masses, currents, and their variability, we used the spiciness frequency averaged in the first 200 m, estimated
 343 following the methods described in Strehl et al. (2024) implementing Equation (5). For this analysis we used the
 344 hydrographic dataset in Brakstad et al (2023). The distribution shown in Figure 8 clearly reveals a southern (northern) side
 345 where the temperature (salinity) dominates the spiciness and hence marking clear α -ocean regimes, while the northern part
 346 has salinity dominated regions associated with β -ocean. These areas largely correspond with the distribution of AW versus
 347 PSW/PSWw (See Fig. 2 for T-S definitions).



348

349

Figure 8: Mean upper 200m spice frequency for the region of study showing the α -ocean (red) and β -ocean (blue) regions for the periods of 1980-2000 and 2000-2020 and the four main seasons JFM (a,b), AMJ (c,d), JAS (e,f) and OND (g,h). The Brakstad et al (2023) hydrographic dataset is used for this calculation.

351

352

The seasonal distribution of spice frequency north of Iceland agrees with the seasonal behavior of the NIIC described in Casanova-Masjoan et al. (2020) where the NIIC surface extension in winter and spring remains constrained to the northwestern side of Iceland due to the cold southeast surface imprint of the EIC. Then in summer, the NIIC expands northeastward, reaching all the way to the eastern side of Iceland and the northernmost station at the SI transect and constraining the polar water between the northern end of the Kolbeinsey Ridge and the Greenland shelf. Then in fall the NIIC northern extension narrows but is still able to surround Iceland. It is noteworthy that a clear increase in coverage of the α -ocean, mainly in summer, is observed by comparing the 1980-200 average and the 2000-2010 average.

358

359

6. DISCUSSION AND CONCLUSIONS

360

In this study, we discussed the seasonal and interannual variability of the mixed layer characteristics and the stratification

361 regimes around Iceland by using a long time series of CTD data. Based on our results, we propose the regionalization of
362 the waters around Iceland into three dynamical regions α -ocean, β -ocean, and transition-ocean.

363 The southwestern region is dominated by AW both in winter and summer. Within this region, the winter MLD
364 is the deepest and most variable of the whole study area, with ML's occupied by AW over the whole sampling period.
365 This region is influenced by the dynamics of the Irminger Sea and the Subpolar gyre and has favorable conditions (α -
366 ocean) for winter deep convection driven by heat fluxes to develop deep mixed layers, which agrees with previous
367 studies (Carmack, 2007; Våge et al., 2008; Piron et al., 2016; Stewart and Haine, 2016; Petit et al., 2020). In the
368 Southern region, the ML salinity anomaly was negative over the last 5 years, which is consistent with previous
369 numerical models and Argo observations showing a freshening trend of the North Atlantic (Tesdal et al., 2018;
370 Holliday et al., 2020, Liu et al., 2020). However, since the South of Iceland is an α -ocean, these recent changes have
371 not yet reached or affected the MLD.

372 The northwestern region, which includes the Denmark Strait, is a medley of all the water masses described in this study.
373 In this region there is a confluence of Greenland shelf and slope waters and Iceland Sea origin waters (Harden et al., 2016;
374 Foukal et al., 2020). This includes the NIIC generating an important variability in the water properties due to complex
375 interactions of the regional currents (Lin et al. 2020, Mastropole et al. 2017). The MLD variability over time at the KG6
376 and LB8 stations is moderate (<100m), except for the years 2000, 2007 and 2016 when the ML was anomalously deep. In
377 this region, the stratification is notably year-round dominated by salinity (β -ocean), which is explained by the strong Polar
378 influence of cold and fresh waters transported by the EGC. A broader look into the northwestern side of the basin reveals
379 that this area can be divided at the center of the Denmark Strait into an α -ocean near the Icelandic shelf where the NIIC
380 flows and a β -ocean as we progress towards Greenland (where the LB8 and KG6 stations are located). Near the Icelandic
381 shelf, MLDs are driven mainly by wind-stress, with a secondary contribution of heat fluxes. The T-S properties as well as
382 the MLT anomalies in the northwest region near the Icelandic shelf show that the NIIC waters there are getting warmer and
383 saltier. This agrees with previous studies showing the transformation of the NIIC also accompanied by an increase in its
384 transport with time (Casanova-Masjoan et al., 2020). Even if the α -ocean area is warming, it is not expanding
385 northwestward. Hence, the EGC is acting as a barrier bringing PSW in the area and maintaining the β -ocean state on the
386 northwesternmost side of the Strait.

387 Northeast of Iceland, the ML exhibits intrusions of SW in the winter, while AW is present during the summer. In this
388 region, the stratification changes from β - to α -ocean seasonally. The Kolbeinsey Ridge acts as a barrier where we find the
389 eastward penetration of the EIC bringing fresh waters (PSWw) from the East Greenland Current (Macrander et al., 2014;
390 Casanova-Masjoan et al., 2020). In summer, the NIIC expands northeastward, bringing AW into the area and changing the
391 stratification regime to α . Hence, the mixed layer waters show important seasonal variability. They range from maximum
392 temperature below 2 °C in winter to over 10 °C in summer. This is also the only region where a significant warming decadal
393 trend emerges over the interannual variability and progressively results in a stronger α -ocean. This agrees with the AW
394 warming observed in Casanova-Masjoan et al. (2020) and with the northward progression of AW named as 'Atlantification'
395 described by Polyakov et al. (2017). This shift to α -ocean or 'Atlantification' may lead to deeper ML's (Moore et al., 2015;
396 Våge et al., 2022), and the associated deeper convection may increase the potential of this area to contribute to the dense
397 flow carried by the NIJ (Semper et al. 2019).

398 The regionalization proposed in this work, based on hydrographic properties, matches the recently proposed distribution
399 of primary production around Iceland (Richardson and Bendtsen, 2021; Cerfonteyn et al., 2023), supporting the importance
400 of MLD properties for the primary production (Ólafsson, 2003). The induced alterations on primary production can lead to

ecosystem changes. For example, Iceland has witnessed a rapid increase in the population of mackerel, a relatively warm-water fish, since 2006 (Astthorsson et al., 2012; Campana et al., 2020) starting from the Southeast towards the north and recently they have been reported almost all around the country. This migration is consistent with our observations of both, the increase in surface temperatures, *i.e.*, northward shift of warmer isotherms over the Iceland Faroe Ridge (de Marez et al., 2025), and the increase of temperatures within the ML in the same regions over the last decade, which may establish new pathways for entire ecosystems.

The long time series investigated here revealed important interannual oscillations of the ML properties. Four main features are to be highlighted: (i) We do not observe any linear trend in the MLD, which is rather subjected to strong interannual variability (ii) Except for the southern stations, influenced by the subpolar gyre, the interannual variability was not correlated with the NAO. For example, FX9 shows a significant negative of MLT with the NAO ($R=-0.41$ and $p\text{-value} < 0.03$). (iii) The linear fit indicates significant (at 95%) warming trends in the MLT of most of the stations in winter, with the maximum trend of $0.08\text{ }^{\circ}\text{C}/\text{year}$ at SI8 resulting in approximately $2.2\text{ }^{\circ}\text{C}$. This agrees with previous studies (Sarafanov, 2009) showing that the northern part of the North Atlantic (South of Iceland) is strongly dominated by atmospheric interannual to decadal variability, particularly, where AW is present. The exception here is the Northeastern region of Iceland where we observe a clear warming trend of the ML (2010-2020). (iv) We observe an ‘Atlantification’ expressed as a northeastward progression of the α -ocean state. This progression will highlight the role of the northeastern area of Iceland as a convective zone where deep water could be formed and contribute to the NIJ.

AUTHOR CONTRIBUTIONS

Conceptualization, ARA, MDPH and EP; methodology, ARA, EP and MDPH; software, ARA and AP; formal analysis, ARA, EP, TM, CdM and MDPH; investigation, ARA, EP and MDPH, AM; data acquisition, SRÓ and AM; data curation, SRÓ and AM; writing—original draft preparation, ARA, EP and MDPH; writing—review and editing, SRÓ, AM and SJ, TM; visualization, ARA and EP; project administration, SRÓ; funding acquisition, ARA and SRÓ. All authors have read and agreed to the published version of the manuscript.

FUNDING

ARA has been supported by HM Queen Margrethe II’s and Vigdís Finnbogadóttir’s Interdisciplinary Research Centre on Ocean, Climate and Society (ROCS) under grant no. 158-4223. Support for this work was also provided by the European Union’s Horizon 2020 research and innovation programme under grant no. 727852, Blue-Action project (AM and SJ). This work has been supported by the FAR-DWO (PID2020-114322RBI00) project from the Spanish Ministry of Research.

ACKNOWLEDGMENTS

We are grateful for the invaluable cooperation we have had with the crews of the Icelandic research vessels Bjarni Sæmundsson and Árni Friðriksson and to the many people at the Marine Research Institute that have contributed to the hydrographic observations over the years. ARA and MDPH would like to dedicate this paper to the memory of Maria Casanova-Masjoan.

436 **Table 1.** Characteristics for the representative stations for each typical surveyed section. The representative ocean currents
 437 at each section are also shown: North Icelandic Irminger Current (NIIC), Irminger Current (IC), East Greenland Current
 438 (EGC), North Icelandic Jet (NIJ), East Icelandic Current (EIC), and North Atlantic Current. (NAC).

439
 440

Station	Depth, m	Lon	Lat	Oceanic region	Significant currents
Faxaflói (FX9)	1010	-27.98	64.35	Subpolar North Atlantic	IC
Látrabjarg (LB8)	658	-27.050	66.083	Denmark Strait	NIIC, EGC, DSO
Kögur (KG6)	980	-23.933	67.583	Western Iceland Sea	EGC, DSO
Hornbanki (HB6)	612	-21.583	67.50	Western Iceland Sea	NIIC, NIJ
Síglunes (SI8)	1023	-18.83	68.00	Kolbeinsey Ridge	NIIC, EGC, EIC, NIJ
Langanes NE (LN6)	1850	-12.66	68.00	Iceland Sea	EIC
Langanes E (LA8)	1251	-9.00	66.37	Iceland Sea	EIC
Krossanes (KR6)	1419	-9.00	65.00	Iceland Sea/ North Atlantic	EIC, NAC
Stokksnes (ST5)	1153	-13.66	63.66	North Atlantic	NAC
Selvogsbanki (SB5)	1006	-21.48	62.98	North Atlantic	IC

441
 442
 443
 444

Table 2. Main water masses definitions for the region of study (Rudels et al., 2005; Våge et al., 2011)

Water mass	Potential Temperature (θ)	Salinity	Potential density (σ_0 , kg m^{-3})
Surface Water(SW)	$> 3^\circ\text{C}$	-	$\sigma_0 < 27.70$
Warm Polar Surface Water (PSW _w)	$0^\circ\text{C} \leq \theta < 3^\circ\text{C}$	-	$\sigma_0 < 27$
Polar Surface Water (PSW)	$< 0^\circ\text{C}$,	-	$\sigma_0 < 27.70$

Atlantic Water(AW)	$> 3^{\circ}C$	> 34.9	-
Atlantic-origin Overflow Water (AtOW)	$0^{\circ}C \leq \theta < 3^{\circ}C$	-	$\sigma_0 \geq 27.8,$ $\sigma_{0.5} < 30.44$
Polar intermediate Water (PIW)	$0^{\circ}C$	≤ 34.676	$\sigma_0 > 27.70,$
Arctic-origin Overflow Water (ArOW)	$< 0^{\circ}C$	-	$\sigma_0 > 27.8,$ $\sigma_{0.5} < 30.44$
Nordic Seas Deep Water (NDW)	$< 0^{\circ}C$	-	$\sigma_{0.5} \geq 30.44$

445
446
447
448
449
450
451
452
453
454
455
456
457
458
459
460
461
462
463
464
465

466

467 **References**

- 468 Astthorsson, O. S., Valdimarsson, H., Gudmundsdottir, A., and Oskarsson, G. J.: Climate-related variations in the
469 occurrence and distribution of mackerel (*Scomber scombrus*) in Icelandic waters, *ICES J. Mar. Sci.*, 69, 1289–1297, 2012.
- 470 Athanase, M., Provost, C., Perez-Hernández, M. D., Sennechael, N., Bertosio, C., Artana, C., et al.: Atlantic water
471 modification north of Svalbard in the Mercator physical system from 2007 to 2020, *J. Geophys. Res.: Oceans*, 125,
472 e2020JC016463, <https://doi.org/10.1029/2020JC016463>, 2020.
- 473 Bachman, S. D., Taylor, J., Adams, K., and Hosegood, P.: Mesoscale and submesoscale effects on mixed layer depth in
474 the Southern Ocean, *J. Phys. Oceanogr.*, 47, 2173–2188, 2017.
- 475 Bindoff, N. L., Cheung, W. W., Kairo, J. G., Arístegui, J., Guinder, V. A., Hallberg, R., et al.: Changing ocean, marine
476 ecosystems, and dependent communities, *IPCC Special Report on the Ocean and Cryosphere in a Changing Climate*, 477–
477 587, 2019.
- 478 Brakstad, A.: *Hydrographic and Geochemical Observations in the Nordic Seas Between 1950 and 2019*, University of
479 Bergen, 2023b.
- 480 Bersch, M.: North Atlantic Oscillation–induced changes of the upper layer circulation in the northern North Atlantic Ocean,
481 *J. Geophys. Res.*, 107(C10), 3156, <https://doi.org/10.1029/2001JC000901>, 2002.
- 482 Campana, S. E., Stefansdottir, R. B., Jakobsdottir, K., and Solmundsson, J.: Shifting fish distributions in warming sub-
483 Arctic oceans, *Sci. Rep.*, 10, 1–14, 2020.
- 484 Carmack, E. C.: The alpha/beta ocean distinction: A perspective on freshwater fluxes, convection, nutrients and
485 productivity in high-latitude seas, *Deep Sea Res. Part II: Top. Stud. Oceanogr.*, 54, 2578–2598, 2007.
- 486 Carton, J. A., Grodsky, S. A., and Liu, H.: Variability of the oceanic mixed layer, 1960–2004, *J. Climate*, 21, 1029–1047,
487 2008.
- 488 Casanova-Masjoan, M., Perez-Hernández, M. D., Pickart, R. S., Valdimarsson, H., Ólafsdóttir, S., Macrander, A., et al.:
489 Along-stream, seasonal, and interannual variability of the North Icelandic Irminger Current and East Icelandic Current
490 around Iceland, *J. Geophys. Res.: Oceans*, 125, e2020JC016283, <https://doi.org/10.1029/2020JC016283>, 2020.
- 491 Cerfonteyn, M., Groben, R., Vaulot, D., et al.: The distribution and diversity of eukaryotic phytoplankton in the Icelandic
492 marine environment, *Sci. Rep.*, 13, 8519, <https://doi.org/10.1038/s41598-023-35516-w>, 2023.
- 493 Dai, A., Luo, D., Song, M., and Liu, J.: Arctic amplification is caused by sea-ice loss under increasing CO₂, *Nat. Commun.*,
494 10, 1–13, 2019.
- 495 de Boyer Montegut, C., Madec, G., Fischer, A. S., Lazar, A., and Iudicone, D.: Mixed layer depth over the global ocean:
496 An examination of profile data and a profile-based climatology, *J. Geophys. Res.: Oceans*, 109,
497 <https://doi.org/10.1029/2004JC002378>, 2004.
- 498 de Marez, C., Ruiz-Angulo, A., & Gula, J. Mesoscale induced vertical fluxes over the Iceland-Faroe ridge. *Geophysical*
499 *Research Letters*, 52(13), 2025.
- 500 Feucher, C., Portela, E., Kolodziejczyk, N., & Thierry, V. Subpolar gyre decadal variability explains the recent
501 oxygenation in the Irminger Sea. *Communications Earth & Environment*, 3(1), 279, 2022.
- 502 Foukal, N. P., Gelderloos, R., and Pickart, R. S.: A continuous pathway for fresh water along the east Greenland shelf, *Sci.*
503 *Adv.*, 6, eabc4254, 2020.

504 Hafrannsóknastofnun: Makríll *Scomber scombrus* Stofnmatskýrslur (stock assessment report), Hafrannsóknastofnun,
505 2024, https://www.hafogvatn.is/static/extras/images/mackerel_2024_techreport_is.html.

506

507 Hansen, B., and Østerhus, S.: North Atlantic–Nordic Seas exchanges, *Prog. Oceanogr.*, 45, 109–208, 2000.

508 Harden, B., Renfrew, I., and Petersen, G.: Meteorological buoy observations from the central Iceland Sea, *J. Geophys.*
509 *Res.-Atmos.*, 120, 3199–3208, 2015.

510 Harden, B. E., Pickart, R. S., Valdimarsson, H., Vage, K., de Steur, L., Richards, C., et al.: Upstream sources of the
511 Denmark Strait overflow: Observations from a high-resolution mooring array, *Deep-Sea Res. Pt. I*, 112, 94–112, 2016.

512 Hátún, H., and Chafik, L.: On the recent ambiguity of the North Atlantic Subpolar Gyre Index, *J. Geophys. Res.-Oceans*,
513 123, 5072–5076, 2018.

514 Hátún, H., Chafik, L., and Larsen, K. M. H.: The Norwegian Sea Gyre – a regulator of Iceland-Scotland Ridge exchanges,
515 *Front. Mar. Sci.*, 8, 1001, 2021.

516 Havik, L., Pickart, R. S., Våge, K., Torres, D. J., Thurnherr, A., Beszczynska-Möller, A., et al.: Evolution of the East
517 Greenland Current from Fram Strait to Denmark Strait: Synoptic measurements from summer 2012, *J. Geophys. Res.-*
518 *Oceans*, 122, 1974–1994, 2017.

519 Hersbach, H., Bell, B., Berrisford, P., et al.: The ERA5 global reanalysis, *Q. J. R. Meteorol. Soc.*, 146, 1999–2049,
520 <https://doi.org/10.1002/qj.3803>, 2020.

521 Holt, J., Schrum, C., Cannaby, H., Daewel, U., Allen, I., Artioli, Y., et al.: Potential impacts of climate change on the
522 primary production of regional seas: A comparative analysis of five European seas, *Prog. Oceanogr.*, 140, 91–115, 2016.

523 Holte, J., Talley, L. D., Gilson, J., and Roemmich, D.: An Argo mixed layer climatology and database, *Geophys. Res. Lett.*,
524 44, 5618–5626, 2017.

525 Ingvaldsen, R. B., Assmann, K. M., Primicerio, R., Fossheim, M., Polyakov, I. V., and Dolgov, A. V.: Physical
526 manifestations and ecological implications of Arctic Atlantification, *Nat. Rev. Earth Environ.*, 2, 874–889, 2021.

527 Jónsson, S.: The circulation in the northern part of the Denmark Strait and its variability, *ICES CM*, 50, 1999.

528 Jónsson, S., and Briem, J.: Flow of Atlantic water west of Iceland and onto the North Icelandic shelf, 2003.

529 Jónsson, S., and Valdimarsson, H.: Water mass transport variability to the North Icelandic shelf, 1994–2010, *ICES J. Mar.*
530 *Sci.*, 69, 809–815, <https://doi.org/10.1093/icesjms/fss024>, 2012.

531 Kohler, J., Serra, N., Bryan, F. O., Johnson, B. K., and Stammer, D.: Mechanisms of mixed-layer salinity seasonal
532 variability in the Indian Ocean, *J. Geophys. Res.-Oceans*, 123, 466–496, 2018.

533 Li, G., Cheng, L., Zhu, J., Trenberth, K. E., Mann, M. E., and Abraham, J. P.: Increasing ocean stratification over the past
534 half-century, *Nat. Clim. Chang.*, 10, 1116–1123, 2020.

535 Liu, C., Liang, X., Chambers, D. P., and Ponte, R. M.: Global patterns of spatial and temporal variability in salinity from
536 multiple gridded Argo products, *J. Clim.*, 33, 8751–8766, 2020.

537 Logemann, K., Ólafsson, J., Snorrason, A., Valdimarsson, H., and Marteinsdóttir, G.: The circulation of Icelandic waters
538 – a modelling study, *Ocean Sci.*, 9, 931–955, 2013.

539 Lozier, M. S., Li, F., Bacon, S., Bahr, F., Bower, A. S., Cunningham, S., et al.: A sea change in our view of overturning in

540 the subpolar North Atlantic, *Science*, 363, 516–521, 2019.

541 Macrander, A., Valdimarsson, H., and Jonsson, S.: Improved transport estimate of the East Icelandic Current 2002–2012,
542 *J. Geophys. Res.-Oceans*, 119, 3407–3424, 2014.

543 Mastropole, D., Pickart, R. S., Valdimarsson, H., Våge, K., Jochumsen, K., and Girton, J.: On the hydrography of Denmark
544 Strait, *J. Geophys. Res.-Oceans*, 122, 306–321, 2017.

545 Mauritzen, C.: Production of dense overflow waters feeding the North Atlantic across the Greenland-Scotland Ridge. Part
546 1: Evidence for a revised circulation scheme, *Deep-Sea Res. Pt. I*, 43, 769–806, 1996.

547 Moore, G. W. K., Våge, K., Pickart, R. S., & Renfrew, I. A. (2015). Decreasing intensity of open-ocean convection in the
548 Greenland and Iceland seas. *Nature Climate Change*, 5(9), 877–882.

549 Ólafsson, J.: Winter mixed layer nutrients in the Irminger and Iceland seas, *ICES Mar. Sci. Symp.*, 219, 329–332, 2003.

550 Intergovernmental Panel on Climate Change (IPCC): Special report on the ocean and cryosphere in a changing climate,
551 2019.

552 Ólafsdóttir, A. H., Utne, K. R., Jacobsen, J. A., Jansen, T., Óskarsson, G. J., Nøttestad, L., Elvarsson, B. Þ., Broms, C.,
553 and Slotte, A.: Geographical expansion of Northeast Atlantic mackerel (*Scomber scombrus*) in the Nordic Seas from 2007
554 to 2016 was primarily driven by stock size and constrained by low temperatures, *Deep-Sea Res. Pt. II*, 159, 152–168, 2019.

555 Østerhus, S., Woodgate, R., Valdimarsson, H., Turrell, B., De Steur, L., Quadfasel, D., Olsen, S. M., Moritz, M., Lee, C.
556 M., Larsen, K. M. H., and Jónsson, S.: Arctic Mediterranean exchanges: a consistent volume budget and trends in transports
557 from two decades of observations, *Ocean Sci.*, 15, 379–399, 2019.

558 Perez, F. F., Ólafsson, J., Olafsdóttir, S. R., Fontela, M., and Takahashi, T.: Contrasting drivers and trends of ocean
559 acidification in the subarctic Atlantic, *Sci. Rep.*, 11, 1–16, 2021.

560 Perez-Hernández, M. D., Pickart, R. S., Torres, D. J., Bahr, F., Sundfjord, A., Ingvaldsen, R., et al.: Structure, transport,
561 and seasonality of the Atlantic Water boundary current north of Svalbard: Results from a yearlong mooring array, *J.*
562 *Geophys. Res.-Oceans*, 124, 1679–1698, 2019.

563 Petit, T., Lozier, M. S., Josey, S. A., and Cunningham, S. A.: Atlantic deep water formation occurs primarily in the Iceland
564 Basin and Irminger Sea by local buoyancy forcing, *Geophys. Res. Lett.*, 47, e2020GL091028, 2020.

565 Petit, T., Lozier, M. S., Josey, S. A., and Cunningham, S. A.: Role of air-sea fluxes and ocean surface density on the
566 production of deep waters in the eastern subpolar gyre of the North Atlantic, *Ocean Sci. Discuss.*, 1–21, 2021.

567 Piron, A., Thierry, V., Mercier, H., and Caniaux, G.: Argo float observations of basin-scale deep convection in the Irminger
568 Sea during winter 2011–2012, *Deep-Sea Res. Pt. I*, 109, 76–90, 2016.

569 Polyakov, I. V., Pnyushkov, A. V., Alkire, M. B., Ashik, I. M., Baumann, T. M., Carmack, E. C., et al.: Greater role for
570 Atlantic inflows on sea-ice loss in the Eurasian Basin of the Arctic Ocean, *Science*, 356, 285–291, 2017.

571 Polyakov, I. V., Rippeth, T. P., Fer, I., Alkire, M. B., Baumann, T. M., Carmack, E. C., et al.: Weakening of cold halocline
572 layer exposes sea ice to oceanic heat in the eastern Arctic Ocean, *J. Clim.*, 33, 8107–8123, 2020.

573 Price, J. F., Weller, R. A., and Pinkel, R.: Diurnal cycling – Observations and models of the upper ocean response to diurnal
574 heating, cooling, and wind mixing, *J. Geophys. Res.-Oceans*, 91, 8411–8427, 1986.

575 Renfrew, I. A., Pickart, R. S., Våge, K., Moore, G. W., Bracegirdle, T. J., Elvidge, A. D., et al.: The Iceland Greenland
576 Seas Project, *Bull. Am. Meteorol. Soc.*, 100, 1795–1817, 2019.

577 Reynolds, R. and Banzon, V.: NOAA optimum interpolation 1/4 degree daily sea surface temperature (OISST) analysis,
578 version 2, NOAA Natl. Cent. Environ. Inf., 10, V5SQ8XB5, 2008.

579 Richardson, K. and Bendtsen, J.: Distinct seasonal primary production patterns in the sub-polar gyre and surrounding seas,
580 *Front. Mar. Sci.*, 2021.

581 Rudels, B., Björk, G., Nilsson, J., Winsor, P., Lake, I., and Nohr, C.: The interaction between waters from the Arctic Ocean
582 and the Nordic Seas north of Fram Strait and along the East Greenland Current: Results from the Arctic Ocean-02 Oden
583 expedition, *J. Mar. Syst.*, 55, 1–30, 2005.

584 Sallée, J.-B., Pellichero, V., Akhoudas, C., Pauthenet, E., Vignes, L., Schmidtko, S., et al.: Summertime increases in upper-
585 ocean stratification and mixed-layer depth, *Nature*, 591, 592–598, 2021.

586 Sarafanov, A.: On the effect of the North Atlantic Oscillation on temperature and salinity of the subpolar North Atlantic
587 intermediate and deep waters, *ICES J. Mar. Sci.*, 66, 1448–1454, 2009.

588 Sarmiento, J. L., Hughes, T. M., Stouffer, R. J., and Manabe, S.: Simulated response of the ocean carbon cycle to
589 anthropogenic climate warming, *Nature*, 393, 245–249, 1998.

590 Semper, S., Våge, K., Pickart, R. S., Valdimarsson, H., Torres, D. J., and Jónsson, S.: The emergence of the North Icelandic
591 Jet and its evolution from Northeast Iceland to Denmark Strait, *J. Phys. Oceanogr.*, 49, 2499–2521, 2019.

592 Shepherd, J. G., Brewer, P. G., Oschlies, A., and Watson, A. J.: Ocean ventilation and deoxygenation in a warming world:
593 Introduction and overview, 2017 [Dataset].

594 Skyllingstad, E. D., Samelson, R. M., Simmons, H., Laurent, L. S., Merrifield, S., Klenz, T., and Centurioni, L.: Boundary
595 layer energetics of rapid wind and wave forced mixing events, *J. Phys. Oceanogr.*, 53, 1887–1900, 2023.

596 Stewart, K. D. and Haine, T. W.: Thermobaricity in the transition zones between alpha and beta oceans, *J. Phys. Oceanogr.*,
597 46, 1805–1821, 2016.

598 Strehl, A.-M., Våge, K., Merdrud, S. L. H., and Barreyre, T.: A 70-year perspective on water-mass transformation in the
599 Greenland Sea: From thermobaric to thermal convection, *Prog. Oceanogr.*, 227, 103304, 2024.

300 Swift, J. H., Aagaard, K., and Malmberg, S.-A.: The contribution of the Denmark Strait overflow to the deep North Atlantic,
301 *Deep-Sea Res. Pt. A*, 27, 29–42, 1980.

302 Tesdal, J.-E., Abernathey, R. P., Goes, J. I., Gordon, A. L., and Haine, T. W.: Salinity trends within the upper layers of the
303 subpolar North Atlantic, *J. Clim.*, 31, 2675–2698, 2018.

304 Valdimarsson, H., Astthórsson, O. S., and Pálsson, J.: Hydrographic variability in Icelandic waters during recent decades
305 and related changes in distribution of some fish species, *ICES J. Mar. Sci.*, 69, 816–
306 825, <https://doi.org/10.1093/icesjms/fss027>, 2012.

307 Våge, K., Moore, G. W. K., Jónsson, S., and Valdimarsson, H.: Water mass transformation in the Iceland Sea, *Deep-Sea*
308 *Res. Pt. I*, 101, 98–109, 2015.

309 Våge, K., Papritz, L., Havik, L., Spall, M. A., and Moore, G. W. K.: Ocean convection linked to the recent ice edge retreat
310 along East Greenland, *Nat. Commun.*, 9, 1–8, 2018.

311 Våge, K., Pickart, R. S., Moore, G., and Ribergaard, M. H.: Winter mixed layer development in the central Irminger Sea:
312 The effect of strong, intermittent wind events, *J. Phys. Oceanogr.*, 38, 541–565, 2008.

313 Våge, K., Pickart, R. S., Spall, M. A., Moore, G., Valdimarsson, H., Torres, D. J., et al.: Revised circulation scheme north

314 of the Denmark Strait, *Deep-Sea Res. Pt. I*, 79, 20–39, 2013.

315 Våge, K., Pickart, R. S., Spall, M. A., Valdimarsson, H., Jónsson, S., Torres, D. J., et al.: Significant role of the North
316 Icelandic Jet in the formation of Denmark Strait Overflow Water, *Nat. Geosci.*, 4, 723–727, 2011.

317 Våge, K., Semper, S., Valdimarsson, H., Jónsson, S., Pickart, R. S., & Moore, G. W. K. (2022). Water mass transformation
318 in the Iceland Sea: Contrasting two winters separated by four decades. *Deep Sea Research Part I: Oceanographic Research*
319 *Papers*, 186, 103824.

320 Whitney, M. M. (2025). Icelandic riverine freshwater distribution, offshore export, and alongshelf connectivity. *Estuarine,*
321 *Coastal and Shelf Science*, 319, 109266.

322 Yamaguchi, R. and Suga, T.: Trend and variability in global upper-ocean stratification since the 1960s, *J. Geophys. Res.-*
323 *Oceans*, 124, 8933–8948, 2019.

324

325